Absence seizures and sleep abnormalities in a rat model of *GRIN2B* neurodevelopmental disorder

Katerina Hristova[1*], Melissa C. Fasol[1*], Niamh McLaughlin[1], Sarfaraz Nawaz[1], Mehmet Taskiran[1], Ingrid Buller-Peralta[1], Alejandro Bassi[2], Adrian Ocampo-Garces[2], Javier Escudero[3], Peter C. Kind[1], Alfredo Gonzalez-Sulser[1]

[*]These authors contributed equally to the work.

Author affiliations:

1 Simons Initiative for the Developing Brain, Patrick Wild Centre, Centre for Discovery Brain Sciences, University of Edinburgh, Edinburgh, United Kingdom EH8 9XD.

2 Laboratorio de Sueño y Cronobiología, Facultad de Medicina, Universidad de Chile, Santiago, Chile.

3 School of Engineering, Institute for Imaging, Data and Communications, University of Edinburgh, Edinburgh, United Kingdom EH9 3JL; and Muir Maxwell Epilepsy Centre, University of Edinburgh.

Corresponding Author: Alfredo Gonzalez-Sulser

Simons Initiative for the Developing Brain Fellow
University of Edinburgh
Centre for Discovery Brain Sciences
1 George Square
Edinburgh, EH89JZ
United Kingdom
Tel: (+44) (0)131 651 1903
Email: agonzal2@ed.ac.uk

Keywords: GRIN2B; neurodevelopmental disorder; EEG; absence seizures; sleep

Abbreviations: ASD = autism spectrum disorder; NMDAR = N-methyl-D-aspartate receptor; SWD = spike and wave discharge; REM = rapid eye movement sleep; NREM = non-rapid eye movement sleep.

Abstract

Pathogenic mutations in *GRIN2B* are an important cause of severe neurodevelopmental disorders resulting in epilepsy, autism and intellectual disability. *GRIN2B* encodes the GluN2B subunit of N-methyl-D-aspartate receptors (NMDARs), which are ionotropic glutamate receptors critical for normal development of the nervous system and synaptic plasticity. Here, we characterized a novel *GRIN2B* heterozygous knockout rat model with 24-hour EEG recordings. We found rats heterozygous for the deletion (*Grin2b*$^{+/-}$) had a higher incidence of spontaneous absence seizures than wild-type rats (*Grin2b*$^{+/+}$). Spike and wave discharges, the electrographic correlate of absences seizures, were longer in duration and displayed increased higher overall spectral power in *Grin2b*$^{+/-}$ animals than those in *Grin2b*$^{+/+}$. Heterozygous mutant rats also had abnormal sleep-wake brain state dynamics over the circadian cycle. Specifically, we identified a reduction in total rapid eye movement sleep and, altered distributions of non-rapid eye movement sleep and wake epochs, when compared to controls. This was accompanied by an increase in overall spectral power during non-rapid eye movement sleep in *Grin2b*$^{+/-}$. The sleep-wake phenotypes were largely uncorrelated to the incidence of spike and wave discharges. We then tested the antiseizure efficacy of ethosuximide, a T-type voltage-gated calcium channel blocker used in the treatment of absence seizures, and memantine, a noncompetitive NMDAR antagonist currently explored as a mono or adjunctive treatment option in NMDAR related neurodevelopmental disorders. Ethosuximide reduced the number and duration of spike and wave discharges, while memantine did not affect the number of spike and wave discharges but reduced their duration. These results highlight two potential therapeutic options for *GRIN2B* related epilepsy. Our data shows the new rat *GRIN2B* haploinsufficiency model exhibits clinically relevant phenotypes. As such, it could prove crucial in deciphering underlying pathological mechanisms and developing new therapeutically translatable strategies for *GRIN2B* neurodevelopmental disorders.

Introduction

GRIN2B pathogenic variants cause multiple neurodevelopmental clinical phenotypes such as epilepsy, autism spectrum disorder (ASD), intellectual disability, sleep impairments and movement abnormalities.[1–5] An estimated 52% of patients with *GRIN2B*-related neurodevelopmental disorder present with severe epilepsy, which is refractory to therapy in half of diagnosed cases.[1] A variety of seizure types occur in patients including infantile spasms and generalized tonic-clonic, focal, and absence seizures.[1,2] De novo *GRIN2B* variants are one of the primary monogenic causes of epileptic encephalopathies, in which epilepsy is thought to worsen neurodevelopmental comorbidities.[1,2,6–8] Dysfunctional sleep is common amongst individuals with GRIN2B mutations, and parental reports indicate at least 60% of patients struggle initiating and maintaining sleep, have breathing irregularities during sleep and suffer with daytime somnolence.[1,5,9] The predicted incidence of *GRIN2B* pathogenic mutations is 5.91 per 100.000 births[10], making it the most prevalent disorder associated with the N-methyl-D-aspartate receptor (NMDAR) coding *GRIN* genes.

NMDARs are sodium, potassium and calcium permeable tetrameric ligand-gated ion channels, which play a critical role in glutamatergic transmission, synaptic plasticity and the development of the nervous system.[11,12] NMDARs are composed of two obligate glycine binding GluN1 subunits and two GluN2 or GluN3 subunits, which bind to glutamate. There are four paralogs for GluN2 (GluN2(A-D)), which display differential expression profiles across development and result in differential channel activity dynamics.[11,12]

GRIN2B encodes GluN2B, which is highly expressed in prenatal and early postnatal periods.[11,12] Later in development the expression of GluN2A, which is encoded by *GRIN2A*, is increased. GluN2B containing receptors have a lower open probability, slower deactivation kinetics and an increased sensitivity to glutamate and glycine compared to GluN2A containing receptors.[12,13] In the context of neurodevelopmental disorders, rodent in vitro data demonstrates that pathogenic *GRIN2B* variants alter NMDAR function[14], neuronal migration[15], dendrite morphogenesis[16,17] and synaptic density[16,18], which likely contribute to the aberrant circuit properties that manifest in *GRIN2B*-related neurodevelopmental disorders.

To test the role of GluN2B on brain network function and the sleep-wake cycle we performed in vivo chronic wireless EEG recordings in a novel rat model of *GRIN2B* haploinsufficiency. We identify spontaneously occurring absence seizures, abnormal sleep-wake brain state patterns, and altered spectral properties in mutant animals. We also test the effects of clinically relevant pharmacological treatments on absence seizures.

Materials and methods

Animals

All animal procedures were undertaken in accordance with the University of Edinburgh animal welfare committee regulations and were performed under a United Kingdom Home Office project license. Long Evans Grin2b heterozygous knockout rats were generated by the Medical College of Wisconsin gene Editing Rat Resource Center with support from the Simons Foundation Autism Research Initiative (LE-Grin2bem1Mcwi, RRID:RGD_14394515), and *GRIN2B* heterozygous knockouts are hereafter referred to as *Grin2b*$^{+/-}$, while wild-type littermates are *Grin2b*$^{+/+}$. Pups were bred in-house and weaned from their dams at postnatal day 22. They were subsequently housed in mixed genotype cages with wild-type littermates (two to six rats per cage) with a 12-hour/12-hour light–dark cycle with ad libitum access to

water and food. Following surgery, animals were single housed. Rats were genotyped by polymerase chain reaction.

Synaptosome preparation

Adult *Grin2b*$^{+/+}$ (one male, five female) and *Grin2b*$^{+/-}$ (six male) rats were anesthetised with isoflurane and decapitated. The hippocampus and somatosensory cortex from each hemisphere were quickly dissected in slushy PBS 1X, snap frozen and stored at -80 °C. The discontinuous Percoll-density gradient (23% bottom, 10% middle, 3% uppermost) was made prior to homogenisation on the preparation day. The tissue was quickly thawed at 37 °C and homogenized in ice-cold homogenisation buffer (1x sucrose/EDTA, pH7.4) using 5-6 up-and-down strokes of a pre-chilled Teflon glass with a motorized homogenizer[19] followed by centrifugation at 2800 rpm for 10 min at 4°C. The supernatant was added gently on 3% Percoll-sucrose (Percoll, P1644, Sigma Aldrich, UK) and centrifuged at 20,000 rpm for 8 min at 4°C. The fraction between 23% and 10% was collected and re-suspended in HEPES-Buffered-Krebs (HBK; in mM: 118.5 NaCl, 4.7 KCl, 1.18 MgSO4, 10 Glucose, 1 Na2HPO4, 20 HEPES, pH 7.4 balanced with Trizma) followed by centrifugation at 13,000 rpm for 15 min at 4°C. The pellet (pure synaptosomes) was dissolved in RIPA buffer with protease inhibitor cocktail (5056489001, Roche, Switzerland) and phosphatase inhibitor cocktails II and III, (P5726 and P0044 respectively, Sigma Aldrich, United Kingdom). Protein concentration was determined with the MicroBCA Assay kit (Pierce BCA protein estimation kit, 23225, ThermoFisher Scientific, United Kingdom).

Western Blot

Approximately 15 µg of synaptosome protein was separated on a precast gradient gel (4-15% Mini-PROTEAN® TGX™ Precast Protein Gels, 4561086, BioRad, United Kingdom) and transferred to nitrocellulose membrane (Amersham™ ProtranÒ Western Blotting Membrane, Nitrocellulose, GE10600002, Sigma Aldrich, United Kingdom) using a Bio-Rad transfer apparatus. Total proteins were stained with a reversible protein stain kit (Memcode 24580, Thermo Fisher Scientific, United Kingdom) according to the manufacturer's instructions. After removing the stain, membranes were blocked with 1:1 TBS1X: Odyssey Blocking Buffer (P/N-927-50003, LI-COR Biotech.) for an hour at room temperature, followed by overnight incubation with primary antibodies (NMDAR2A-1: 1000, #ab169873, Abcam; NMDAR2B-1:1000, #610417, BD Biosciences; PSD95- 1:2000, #76115, Abcam; GluR1- 1:1000, #MAB2263, Millipore) at 4°C. Membranes were washed with TBST1X (0.1% Tween 20), and incubated for an hour at room temperature with secondary antibodies (IRDye 680RD Donkey anti-rabbit IgG- 1:5,000, #P/N 926-68073; IRDye 800CW Donkey anti-mouse IgG - 1:5,000, #P/N 926-32212, LI-COR Biotechnology, United Kingdom). Membranes were washed with TBST1X, dried and digitally scanned using an Odyssey M Imager, LI-COR, UK Ltd. Odyssey software, Licor Image Studio Lite (LICOR Biosciences, United Kingdom) was used to quantify individual bands. Data was normalised to respective total protein and normalised to wild-type levels.

Surgery

Rats were anaesthetised with isoflurane and mounted on a stereotaxic frame (David Kopf Instruments, United States). Animals received subcutaneous Rimadyl Small Animal Solution (5 mg/kg, Zoetis, United states) for analgesia and 2.5 ml of sterile 0.9% saline for rehydration.

For surface EEG grid implantation, two holding screws for structural support (4 mm rostral, ± 0.5 mm lateral relative to bregma) and one ground screw over the cerebellum (-11.5 mm rostral, 0.5 mm lateral relative to bregma) (Yahata Neji, M1 Pan Head Stainless Steel Cross, RS Components, United Kingdom) were attached. 16-channel EEG surface grids with two

integrated electromyogram (EMG) leads (Custom H16-Rat EEG16_Functional-NeuroNexus, United States) were placed over the skull with the EEG surface grid plus-symbol reference point aligned over bregma. Silver paint was used for connecting the ground screw with the grid. The implant was fixed to the skull using dental cement (Simplex Rapid, Kemdent, United Kingdom). A 21 G sterile needle tip was used to guide EMG wires (2.5 cm in length with 0.5 cm striped of insulation) into the neck muscle, after which the incision was sutured. Fifteen *Grin2b*$^{+/-}$ (eight male, seven female) and nine *Grin2b*$^{+/+}$ (three male, six female) animals were recorded and used for analyses.

For 2-channel EEG recordings for pharmacology experiments, bilateral screws were implanted to provide structural support (4 mm rostral, ± 0.5 mm lateral relative to bregma). Two ground screws were attached over the cerebellum (-11.5 mm rostral, ± 0.5 mm lateral relative to bregma), and two bilateral electrode screws were fixed over the primary somatosensory cortex (- 2.5 mm rostral, ± 4.5 lateral relative to bregma) (Yahata Neji, M1 Pan Head Stainless Steel Cross, RS Components). Electrode and ground screws were connected to an electronic interface board (EIB-16, Neuralynx) via silver wire soldered to each component (Teflon Coated Silver Wire, World Precision Instruments). The implant was fixed to the skull using dental cement (Simplex Rapid, Kemdent, United Kingdom). Twelve *Grin2b*$^{+/-}$ (ten male, two female) and five *Grin2b*$^{+/+}$ (one male, four female) animals were recorded and used in pharmacology experiments.

EEG recording

All animals were given a minimum of 1-week post-surgery recovery before recordings. Rats were habituated to the recording room for at least 24 hours. Animals were briefly anaesthetised with isoflurane to connect implants to wireless amplifiers, and subsequently recorded for 72 to 96 hours using the TaiNi wireless multichannel recording system (Tainitec, United Kingdom)[20] at a sampling rate of 250.4Hz. Experimenters were blind to genotype.

Absence seizure detection and sleep-wake scoring

The electrographic correlate of absence seizures, spike and wave dischargers (SWDs), were characterized by periodic high-amplitude oscillations between 5 and 10 Hz[21], which coincided with a spontaneous arrest of animal movement. We utilized a previously published automatic SWD detector algorithm to quantify SWDs.[22,23] Spectral analysis allowed for the identification of harmonic peaks in the SWD frequency range. The code used for analysis is available at https://github.com/Gonzalez-Sulser-Team/SWD-Automatic-Identification.

A custom-made automated sleep scoring algorithm, based on a previously published method[24], was used to assign epochs to one of three brain states: wake, rapid eye movement (REM) sleep and non-rapid eye movement (NREM) sleep. Traces from EEG channels overlying S1 on either brain hemisphere and the two EMG channels were visually inspected for excessive movement artefacts. The EEG and EMG channels with less artefacts were chosen for analysis and if both EEG or EMG traces had similar noise levels, one channel for each modality was randomly chosen for analysis. Spectral logarithmic EEG and EMG power was calculated for non-overlapping 5 second epochs in the 0.2-125 Hz frequency range using the *multitaper* package[25] for R[26], using a non-overlapping window-size of 0.2 Hz half-time and bandwidth product of three. Each epoch was plotted in a three-dimensional metric space with values representing theta EEG power (maximum of the power in the 6.0 – 8.2 Hz range), delta and sigma power (1 - 20 Hz mean power, excluding the theta range), and neck muscle activity power (EMG power in the 60–90 Hz range). For clustering into brain states, centroids were estimated using an iterative algorithm that maximizes the local density by segregating the epochs based on the following characteristics: NREM sleep displayed high delta and sigma

power with low EMG power, REM sleep displayed high theta power and low EMG power, and wake displayed high EMG power and low delta and sigma power. The distribution of clusters around the estimated centroid were approximated by Gaussian models assuming ellipsoidal shapes. The covariance matrix of the Gaussian models was used to calculate the Mahalanobis distance from a given epoch to each cluster. The epochs are assigned to a sleep stage according to a minimum Mahalanobis distance to the respective cluster.

All epochs identified to contain SWDs were classed separately from the other three brain states. An additional peak detection algorithm[27] was required to identify SWDs during wake epochs. This algorithm utilises z-scores to identify peaks by calculating a moving mean and flagging datapoints that deviate from the moving mean by a given threshold. If peaks were identified in both 5 - 9 Hz and 10 -18 Hz, this was indicative of the presence of harmonics, which are evident in SWD epochs. After automated scoring of all additional SWD epochs the sleep quantification was adjusted accordingly. SWD distribution across wake and REM was determined by evaluating the first 5 second epoch prior to a seizure occurring, while the first 30 seconds (six epochs) prior were used to assess SWD initiation in NREM and wake-NREM transitions.

After initial brain state scoring, further processing was performed on the data to remove epochs with excessive noise. A bandpass Butterworth filter (0.2 – 100 Hz) was applied to the full-length raw data. 5 second epochs were extracted from the filtered recording and discarded if any data point exceeded 3000mV, which was beyond the range of physiological activity.

To calculate the power spectral density, brain state epoch averages were Hanning-tapered and Fourier transformed using the SciPy welch method (with 50% overlapping windows). The spectral slope, a regression-based fitting measurement which describes the rate of change of the EEG power spectra, was calculated between 1 - 48 Hz using the NumPy *polyfit* function.[28] Epochs that were outside of the visually selected threshold of -5 $\log_{10}(mV^2)/Hz$ for the spectral slope and 500 mV for the spectral offset were removed from further analyses.

We validated automated sleep scoring performance by comparing the automatically generated vigilance state output with visual EEG state scoring of identical 5 second epochs. Researchers visually scoring were blind to automated output. We manually scored 4 hours of EEG in seventeen animals, between 10:00 – 14:00 o'clock, when approximately equal distributions of wake, NREM and REM epochs were observed. Percent agreement and Cohen's kappa were calculated to assess interrater reliability between visual and automatic scoring of brain states.[29] In our datasets, agreement between visual and automatic scoring was 88.1%, 87.5% and 95% for REM, NREM and wake states respectively. Overall agreement between the scoring methods was 90.8%. The kappa coefficient was 0.83 (± 0.002 SE) (Supplementary Fig. 1, Supplementary Table 1).

SWDs and brain state data was analysed over 48 hours and values per hour were averaged over two days starting at zeitgeber time 07:00 am of the day after connection, under a 12-hour/12-hour light–dark schedule. The automated sleep scoring code is available at https://github.com/Gonzalez-Sulser-Team/AUTOMATIC-SLEEP-SCORER.

Pharmacology experiments

For pharmacology experiments, time-matched 2-hour periods from 11:00 to 13:00 o'clock across days, were used to analyse the effects of pharmacological treatments on SWDs. Drugs were dissolved in 1 ml of sterile 0.9% saline and rats received treatment based on their weight. Animals received either intraperitoneal ethosuximide (100 mg/kg, Merck, Germany), memantine (5 mg/kg, Enzo Life Sciences, United States), or saline as a vehicle control on separate days, between baseline and washout days. There were 24 hours in between each

experimental day (baseline, drug and washout). Experimenters were blinded to treatment, and the order of treatments was counterbalanced to minimize the risk of synergistic effects between drugs (Fig. 6A).

Statistical analyses

Normality and homoscedasticity for all data were estimated by Shapiro–Wilk and Levene's tests (rejection value set at < 0.05), and based on these, comparisons between genotypes were made using two-sample unpaired t-test, Welch's two-sample t-test or Wilcoxon rank sum test. One-way, two-way or mixed effects ANOVA tests were performed where more than two groups were compared, for factorial analyses (genotype and sex) and where multiple measures were taken from the same subjects; wherever appropriate, these were followed by *post hoc* Tukey's multiple comparisons. Pearson correlation was used to test the relationship of SWDs with brain state abnormalities. Analyses were conducted in R[26], RStudio[30], using the *ggplot2*, *car* and *lmerTest* packages [31–33]. All the data in the figures were presented as mean ± SEM, and $P < 0.05$ was considered as significant and indicated with $^{*}P < 0.05$, $^{**}P < 0.01$, $^{***}P < 0.001$, $^{****}P < 0.0001$.

Funding

The Simons Initiative for the Developing Brain, Patrick Wild Centre, The Carnegie Trust for The University of Scotland Research Initiative Award RIG01249, Royal Society Seed Corn RGS\R1\221112, and a Wellcome Trust Institutional Support Fund grant 204804/Z/16/Z.

Author Contributions

Katerina Hristova[1,*], Melissa C. Fasol[1,*], Niamh McLaughlin[1], Sarfaraz Nawaz[1], Mehmet Taskiran[1], Ingrid Buller-Peralta[1], Alejandro Bassi[2], Adrian Ocampo-Garces[2], Javier Escudero[3], Peter C. Kind[1], Alfredo Gonzalez-Sulser[1]

A.G.S., P.C.K and J.E. designed experiments. K.H., S.N. and M.H. performed experiments. K.H., M.C.F., N.M., and S.N. analysed the data. A.G.S., M.C.F., A.B., and A.O.G. developed analysis protocols. K.H. and A.G.S. wrote the manuscript with input from all authors.

Competing Interests.

Authors declare no competing interests.

Results

Gene expression in a novel rat model of GRIN2B neurodevelopmental disorder

We utilized a novel model of *GRIN2B* related neurodevelopmental disorder generated by the Medical College of Wisconsin Gene Editing Rat Resource Centre, in which CRISPR/Cas9 was used to introduce a mutation in the *GRIN2B* gene of Long-Evans rats. Mutant protein expression was confirmed by immunoblotting somatosensory cortex (Fig. 1A) and hippocampus (Supplementary Fig. 2A, Supplementary Fig. 3A-D) homogenates, and found to be located at synapses by immunoblotting of somatosensory and hippocampal synaptosome fractions (Fig. 1B and Supplementary Fig. 2B). Glun2B protein levels in homogenates and synaptosome fractions were reduced by approximately 50% in adult heterozygous mutant ($Grin2b^{+/-}$) rats compared to wild-types ($Grin2b^{+/+}$) in somatosensory cortex and hippocampus (somatosensory cortex homogenate, Two-sample unpaired t-test, $DF = 10$, $T = 5.107$, $P = 0.00046$; synaptosome, Wilcoxon rank sum test, $W = 36$, $P = 0.0051$; hippocampal homogenate, Two-sample unpaired t-test, $DF = 10$, $T = 6.86$, $P = 0.000044$; synaptosome, Two-sample unpaired t-test, $DF = 10$, $T = 3.061$, $P = 0.012$; Fig. 1C and Supplementary Fig. 2C). The expression of GluN2A, GluR1 and PSD95 synaptic proteins in $Grin2b^{+/-}$ rats was

unaffected in the somatosensory cortex (GluN2A homogenate, Two-sample unpaired t-test, *DF* = 10, *T* = 0.3, *P* = 0.77; synaptosome, Two-sample unpaired t-test, *DF* = 10, *T* = 0.46, *P* = 0.66; GluR1 homogenate, Two-sample unpaired t-test, *DF* = 10, *T* = 0.85, *P* = 0.42; synaptosome, Welch's two-sample unpaired t-test, *DF* = 5.46, *T* = 1.27, *P* = 0.26; PSD95 homogenate, Two-sample unpaired t-test, DF = 10, *T* = 2.11, *P* = 0.061; synaptosome, Two-sample unpaired t-test, *DF* = 10, *T* = 0.16, *P* = 0.88; Fig. 1D-F) and the hippocampus (GluN2A homogenate, Two-sample unpaired t-test, *DF* = 10, *T* = -0.38, *P* = 0.71; synaptosome, Two-sample unpaired t-test, *DF* = 10, *T* = -0.025, *P* = 0.98; GluR1 homogenate, Two-sample unpaired t-test, *DF* = 10, *T* = 0.65, *P* = 0.53; synaptosome, Wilcoxon rank sum test, *W* = 10, *P* = 0.23; PSD95 homogenate, Two-sample unpaired t-test, *DF* = 10, *T* = -0.14, *P* = 0.89; synaptosome, Two-sample unpaired t-test, *DF* = 10, *T* = -0.34, *P* = 0.74; Supplementary Fig. 2D-F). Despite the reduction in GluN2B expression, *Grin2b*$^{+/-}$ animals appeared healthy, fertile and indistinguishable from wild-type littermates.

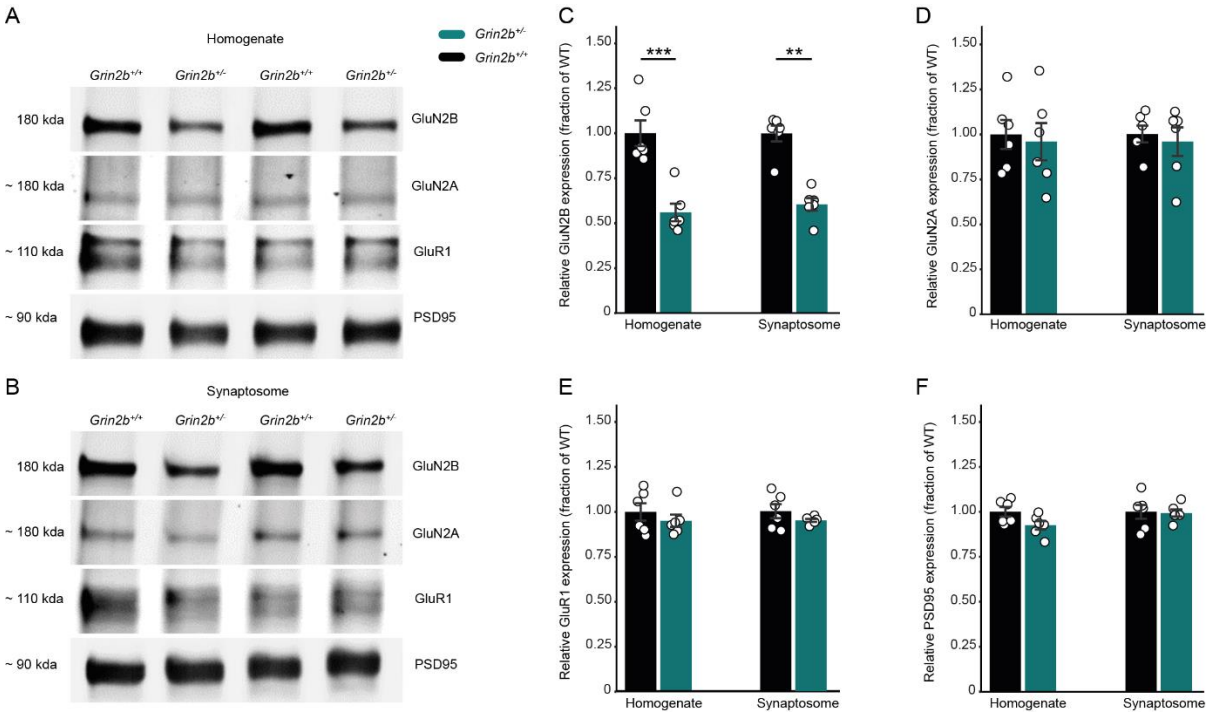

Figure 1 GRIN2B deletion in rats results in reduction of endogenous GluN2B expression in somatosensory cortex. *Representative Western blots of extracts from rat somatosensory brain homogenates (**A**) and synaptosomes (**B**). Bands in the molecular weight range expected for full length GluN2B, GluN2A, GluR1 and PSD95 were detected in homogenates and synaptosomes from wild-type and Grin2b*$^{+/-}$ *animals. (**C**) Quantification of GluN2B protein from homogenates and synaptosomes reveals a significant decrease in Grin2b*$^{+/-}$ *rats (P = 0.00046, P = 0.0051, Two-sample unpaired t-test and Wilcoxon rank sum tests). There was no change in Grin2b*$^{+/-}$ *rats in expression levels of GluN2A P = 0.77, P = 0.66, Two-sample unpaired t-test) (**D**), GluR1 (P = 0.42, P = 0.26, Two-sample unpaired t-test) (**E**), or PSD95 (P = 0.061, P = 0.88, Two-sample unpaired t-test) (**F**). Detailed statistics in text. Bars indicate mean values (mean ± SEM). Points correspond to values from individual rats.*

Absence seizures in *Grin2b*$^{+/-}$ rats

To determine whether heterozygous knockout of *GRIN2B* results in epileptic seizures and if it affects sleep-wake brain states across the circadian cycle, animals were implanted with 14-channel surface electrode grids and EMG electrodes in neck muscles (Fig. 2A). Wireless freely moving 24-hour recordings were performed in the rats' home cages.

Grin2b$^{+/-}$ rats displayed spontaneous behavioural arrests reminiscent of absence seizures which correlated with electrographic SWDs (Fig. 2A). A higher frequency of SWDs was found across the 24-hour period in *Grin2b*$^{+/-}$ animals, although no hour-by-hour differences were found (Mixed effects ANOVA, effect of genotype $F = 55.36$, $DF = 1$, $P < 0.00001$; effect of hour $F = 1.29$, $DF = 23$, $P = 0.16$; hour x genotype $F = 0.97$, $DF = 23$ $P = 0.49$; Fig. 2B). The total number of SWDs over 24 hours was also significantly higher in *Grin2b*$^{+/-}$ rats than in wild-type *Grin2b*$^{+/+}$ littermates (Wilcoxon rank sum test, $W = 4.5$, $P = 0.0002$; Fig. 2C). Furthermore, *Grin2b*$^{+/-}$ rats had a longer average SWD duration than *Grin2b*$^{+/+}$ rats (Two-sample unpaired t-test, $DF = 22$, $T = -5.26$, $P = 0.00003$; Fig. 2C) and the total duration of SWDs was also significantly longer in *Grin2b*$^{+/-}$ animals when compared to *Grin2b*$^{+/+}$ rats (Wilcoxon rank sum test, $W = 5.5$, $P = 0.0002$; Fig. 2C). These results suggest that GRIN2B haploinsufficiency drives the network to a state of increased absence seizure activity.

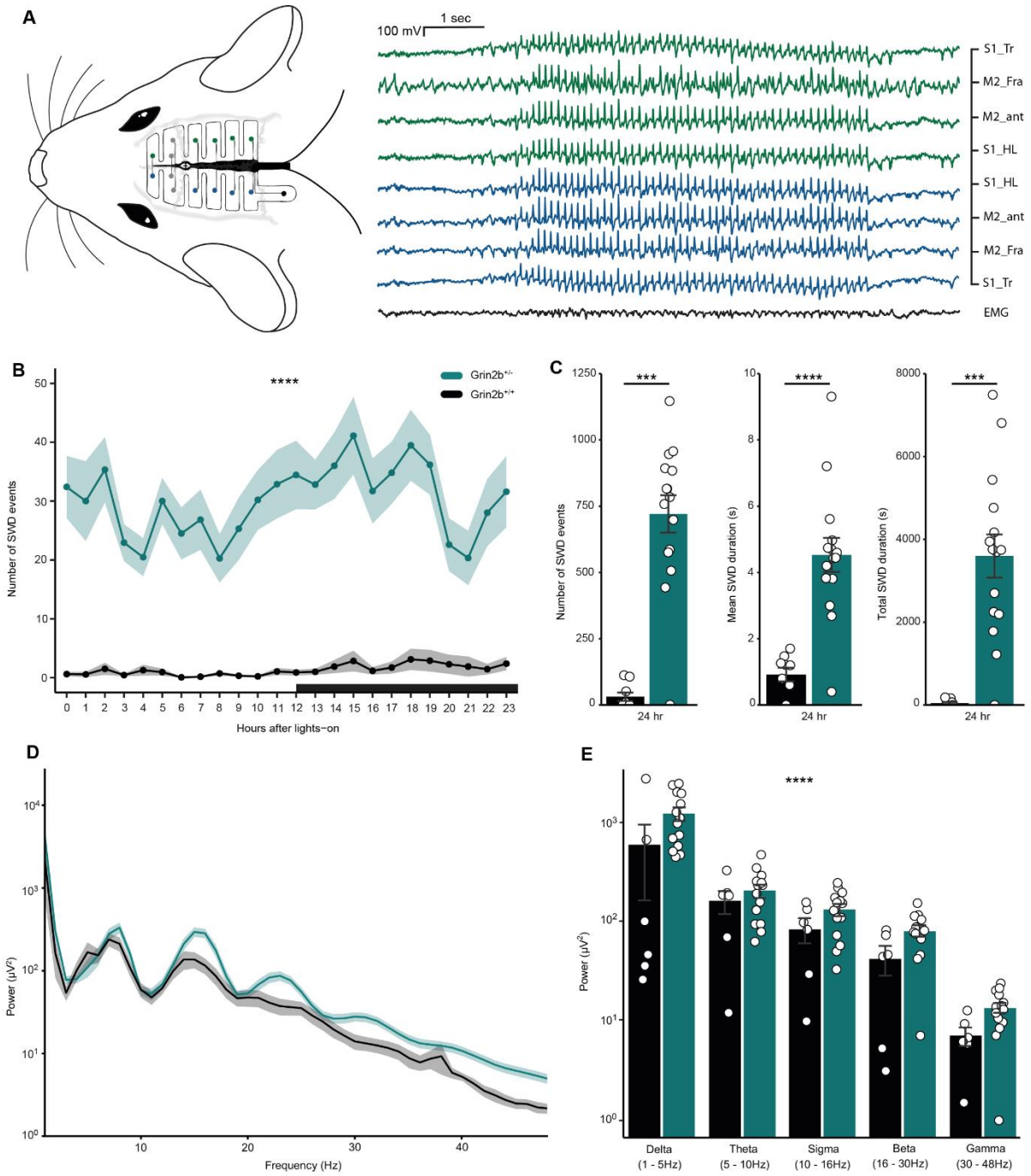

Figure 2 Prevalence and spectral properties of absence seizures in Grin2b$^{+/-}$ animals. *(**A**) Schematic of a 16-channel skull-surface EEG implant illustrating approximate placement of electrodes relative to the skull (left) and representative EEG and EMG voltage traces from bilateral electrode pairs in diagram showing a SWD (right). (**B**) Number of SWD events plotted by hour over the 24-hour light-dark cycle with black bar on x-axis indicating lights off in the animal facility. Grin2b$^{+/-}$ rats had significantly more seizures overall than wild-type littermates in hour-by-hour analysis (genotype P < 0.00001, hour P = 0.16, hour x genotype P = 0.49, Mixed effects ANOVA), (**** = effect from genotype). Points indicate mean values (mean ± SEM). (**C**) Bar plots of total number of SWD events (left), SWD average duration (middle) and total SWD durations (right) across the entire 24 hours with Grin2b$^{+/-}$ rats having significantly higher values (P = 0.0002, P = 0.00003, P = 0.0002, Two-sample unpaired t-test and Wilcoxon rank sum tests). (**D**) Average EEG power spectra for Grin2b+/- rats and wild-type littermates during all SWD epochs across all animals in each group (mean ± SEM). (**E**) Quantification of average power in commonly used frequency bands during SWDs, showing an overall increased spectral power (genotype P < 0.00001, frequency P < 0.0001, genotype x frequency P = 0.12, Two-way ANOVA). Detailed statistics in text. **** = effect from genotype. Bars indicate mean values (mean ± SEM). Points correspond to values from individual rats.*

We performed spectral analysis on SWDs to determine if these differed significantly between genotypes. In SWD epoch averages we found a clear peak in the theta frequency range with a secondary harmonic in both genotypes (Fig. 2D). Spectral power during SWDs in *Grin2*$^{-+/-}$ rats was higher when compared to wild-type littermates although this was not specific to individual frequency bands (Two-way ANOVA, effect of genotype F = 23.99, DF = 1, P < 0.00001; frequency F = 43.36, DF = 4, P < 0.0001; genotype x frequency F = 1.97, DF = 4, P = 0.12; Fig. 2E). The overall increased power in *Grin2b*$^{+/-}$ rats may indicate differences in the underlying mechanisms of SWD generation.

To determine whether male and female *Grin2b*$^{+/-}$ rats have different susceptibility to the occurrence of SWDs, we compared the two sexes. Hour-by-hour SWD analysis was still significantly different between genotypes, but there were no sex differences (Mixed effects ANOVA, effect of hour F = 1.24, DF = 23, P = 0.021; genotype F = 47.83, DF = 1, P < 0.00001; sex F = 0.12, DF = 1, P = 0.73, hour x genotype x sex F = 0.85, DF = 23, P = 0.66; Supplementary Fig. 4A).

Similarly, while there were still significant differences between genotypes, there were no differences between male and female *Grin2b*$^{+/-}$ rats in the total number of SWD events (Two-way ANOVA, effect of sex F = 0.12, DF = 1, P = 0.74; genotype F = 47.663 DF = 1, P < 0.0001; sex x genotype F = 0.2, DF = 1, P = 0.66; Supplementary Fig. 4B), the mean duration of SWDs (Two-way ANOVA, effect of sex F = 0.0002, DF = 1, P = 0.99; genotype F = 23.17, DF = 1, P = 0.0001; sex x genotype F = 0.017, DF = 1, P = 0.89; Supplementary Fig. 4B) or the total time spent in a state of SWDs (Two-way ANOVA, effect of sex F = 0.0001, DF = 1, P = 0.99; genotype F = 22.9, DF = 1, P = 0.0001; sex x genotype F = 0.002, DF = 1, P = 0.96; Supplementary Fig. 4B).

Sleep-wake abnormalities in *Grin2b*$^{+/-}$ rats

We quantified minutes spent in REM, NREM and wake (Fig. 3A-C) to determine if *Grin2b*$^{+/-}$ animals exhibited abnormal sleep-wake patterns as reported in patients.[5] *Grin2b*$^{+/-}$ rats displayed a decrease in REM sleep minutes in hour-by-hour analysis although no significant differences were found in individual hours of the day (Mixed effects ANOVA, effect of hour F = 16.13, DF = 23, P < 0.00001; genotype F = 9.98, DF = 1, P = 0.0045; hour x genotype F = 0.95, DF = 23, P = 0.53; Fig. 3D). *Grin2b*$^{+/-}$ rats spent less total time in REM sleep than wild-type littermate controls (Two-sample unpaired t-test, DF = 22, T = 3.16, P = 0.0045; Fig. 3G),

which was due to a decreased number of REM sleep bouts (Two-sample unpaired t-test, *DF* = 22, *T* = 3.94, *P* = 0.00069; Fig. 3G). Interestingly, the average duration of REM sleep bouts was longer for *Grin2b*$^{+/-}$ animals (Wilcoxon rank sum test, *W* = 33, *P* = 0.043) (Fig. 3G), however, this was insufficient in compensating for the net REM deficit observed.

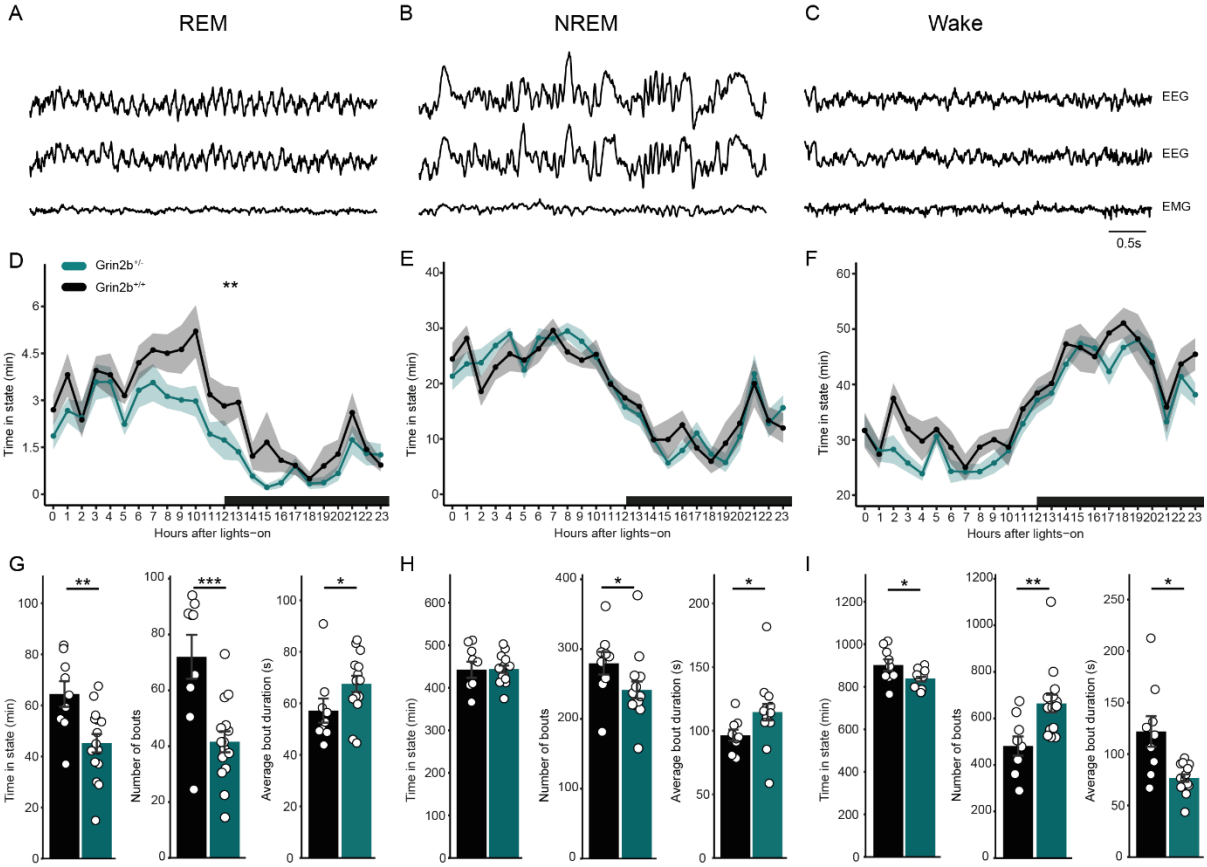

Figure 3 Grin2b$^{+/-}$ animals display sleep-wake abnormalities. *Representative EEG and EMG voltage traces for REM (**A**), NREM (**B**) and wake (**C**). Quantification showing the time spent in REM (**D**), NREM (**E**) and wake (**F**) by hour, across the 24-hour light-dark cycle with black bar on x-axis indicating lights off in the animal facility. Grin2b$^{+/-}$ rats had significantly less REM sleep compared to wild-type littermates on an hour-to-hour basis, while no differences were observed between genotypes in NREM and wake states (REM hour P < 0.00001, genotype P = 0.0045, hour x genotype P = 0.53; NREM hour P < 0.00001, genotype P = 0.93, hour x genotype P = 0.66; wake hour P < 0.00001, genotype P = 0.014, hour x genotype P = 0.84; Mixed effects ANOVA tests), (** = effect from genotype). Points indicate mean values (mean ± SEM). Bar plots showing total time, number of bouts and average bout duration for REM (**G**), NREM (**H**) and wake (**I**) during the full 24 hours (* = P < 0.05, ** = P < 0.01, *** = P < 0.001, unpaired Two-sample t-tests and Wilcoxon rank sum tests specified in results text). Bars indicate mean values (mean ± SEM). Points correspond to values from individual rats.*

In hour-by-hour analysis, both groups spent equivalent amounts of time in NREM sleep (Mixed effects ANOVA, effect of hour *F* = 21.52, *DF* = 23, *P* < 0.00001; genotype *F* = 0.0081, *DF* = 1, *P* = 0.93; hour x genotype *F* = 0.86, *DF* = 23, *P* = 0.66; Fig. 3E). Similarly, there was no difference between *Grin2b*$^{+/-}$ and *Grin2b*$^{+/+}$ rats in the total amount of time spent in NREM over the full 24 hours (Two-sample unpaired t-test, *DF* = 22, *T* = -0.09, *P* = 0.93; Fig. 3H). Nonetheless, *Grin2b*$^{+/-}$ rats demonstrated abnormal NREM distributions when compared to *Grin2b*$^{+/+}$ littermates, as they had less NREM bouts (Wilcoxon rank sum test, *W* = 29.5, *P* =

0.025; Fig. 3H), which where longer in average duration (Wilcoxon rank sum test, W = 26, P = 0.015; Fig. 3H).

Wake minutes were also significantly decreased in *Grin2b*$^{+/-}$ rats, although there were no differences detected in individual hours of the day (Mixed effects ANOVA, effect of hour F = 22.55, DF = 23, P < 0.00001; genotype F = 7.14, DF = 1, P = 0.014; hour x genotype F = 0.71, DF = 23, P = 0.84; Fig. 3F). When compared to wild-type littermates, the total minutes awake were significantly less in *Grin2b*$^{+/-}$ rats (Welch's two-sample unpaired t-test, DF = 10.25, T = 2.26, P = 0.047; Fig. 3I) with mutants having more wake bouts (Wilcoxon rank sum test, W = 18, P = 0.0035; Fig. 3I) of shorter duration (Welch's two-sample unpaired t-test, DF = 8.91, T = 2.97, P = 0.016; Fig. 3I).

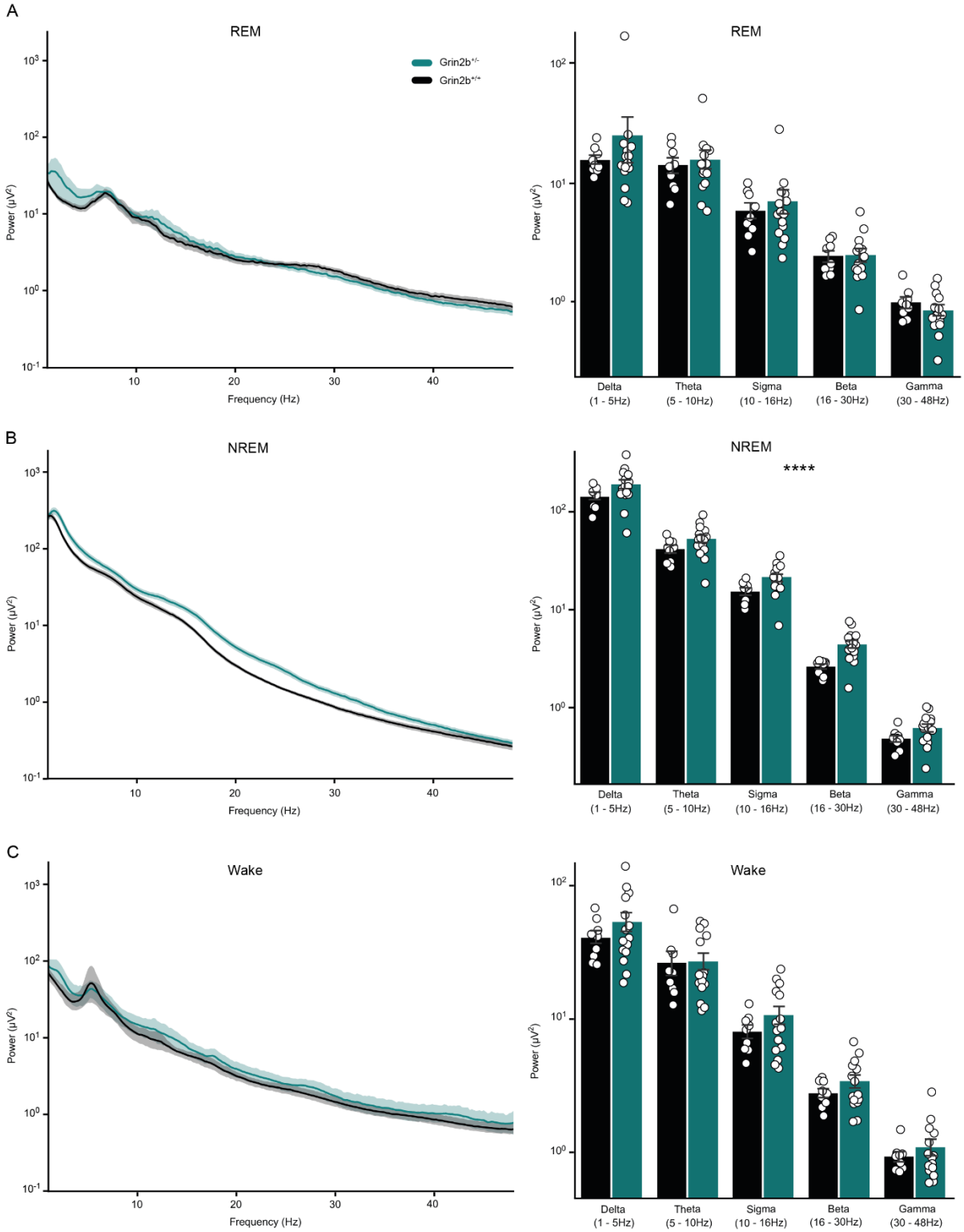

Figure 4 Spectral power is increased in NREM sleep in Grin2b$^{+/-}$ rats. *Average EEG power spectra across wild-type and Grin2b$^{+/-}$ rats (left) and quantification by individual frequency bands (right) during REM (**A**), NREM (**B**) and wake (**C**) epochs. Quantification of average power in specific frequency bands during REM epochs and wake, showed no spectral differences between Grin2b$^{+/-}$ and wild-type animals (REM genotype P = 0.98, frequency P < 0.0001, genotype x frequency P = 0.89; wake genotype P = 0.17, frequency P < 0.00001, genotype x frequency P = 0.98; Two-way ANOVA tests). Spectral power was significantly higher during NREM epochs in Grin2b$^{+/-}$ rats although no significant differences were found in*

*individual frequency bands (genotype P = 0.000023, frequency P < 0.0001, genotype x frequency P = 0.66, Two-way ANOVA), (**** = effect from genotype). Detailed statistics in main text. Bars indicate mean values (mean ± SEM). Points correspond to values from individual rats.*

Sleep states are altered in *Grin2b*$^{+/-}$ rats. However, there were no significant differences between male and female mutant and wild-type animals (for statistical results see Supplementary Table 1) (Supplementary Fig. 5A-F).

We next tested whether *Grin2b*$^{+/-}$ animals had abnormal spectral properties across their sleep-wake cycle. We calculated the average EEG spectral power from one representative channel across all animals and epochs of each brain state. No significant differences were found between *Grin2b*$^{+/-}$ and *Grin2b*$^{+/+}$ rats during REM sleep (Two-way ANOVA, effect of genotype $F = 0.0003$, $DF = 1$, $P = 0.98$; frequency $F = 139.83$, $DF = 4$, $P < 0.00001$; genotype x frequency $F = 0.28$, $DF = 4$, $P = 0.89$; Fig. 4A) and wake (Two-way ANOVA, effect of genotype $F = 1.89$, $DF = 1$, $P = 0.17$; frequency $F = 258.1$, $DF = 4$, $P < 0.00001$; genotype x frequency $F = 0.13$, $DF = 4$, $P = 0.98$, Fig. 4C). However, power was significantly increased across frequency bands in NREM sleep, although there were no statistical differences in specific bands (Two-way ANOVA, effect of genotype $F = 19.61$, $DF = 1$, $P = 0.000023$; frequency $F = 932.18$, $DF = 4$, $P < 0.00001$; genotype x frequency $F = 0.61$, $DF = 4$, $P = 0.66$; Fig. 4B). Grouped together, the above results show that *Grin2b*$^{+/-}$ rats have altered sleep-wake brain state distributions and spectral properties.

Brain state abnormalities in *Grin2b*$^{+/-}$ rats are not correlated with absence seizure activity

The increased SWD activity in *Grin2b*$^{+/-}$ rats may contribute to the altered sleep-wake brain states. We therefore tested whether SWDs preferentially occurred during wake, NREM or REM sleep. Overall, we found seizures predominantly occurred during wake (94.8%), followed by NREM (4.4%) and scarcely during REM sleep (0.5%) (Fig. 5A).

SWDs initiated more frequently during NREM in *Grin2b*$^{+/-}$ rats than in wild-type littermates, while wild-types in contrast had a higher percentage of seizures when awake compared to *Grin2b*$^{+/-}$ animals (Two-way ANOVA, effect of genotype $F = 1$, $DF = 1$, $P = 0.98$; state $F = 5945.056$, $DF = 2$, $P < 0.00001$; genotype x state $F = 10.94$, $DF = 2$, $P = 0.00008$; Tukey *post hoc* test, wake $P = 0.0022$, NREM $P = 0.0011$; Fig. 5A). The increased frequency of *Grin2b*$^{+/-}$ SWDs in NREM sleep prompted us to examine whether the wake-NREM transitional state (Fig. 5B and C), when synchronous subcortical output is increased [34], is linked to SWD occurrence. We tested all SWD epochs identified in NREM and found 24.2% of SWDS in *Grin2b*$^{+/-}$ rats occurred during the wake-NREM transitional period, which was significantly higher than in wild-type littermates at 7.5% (Wilcoxon rank sum test, $W = 20.5$, $P = 0.0052$; Fig. 5C).

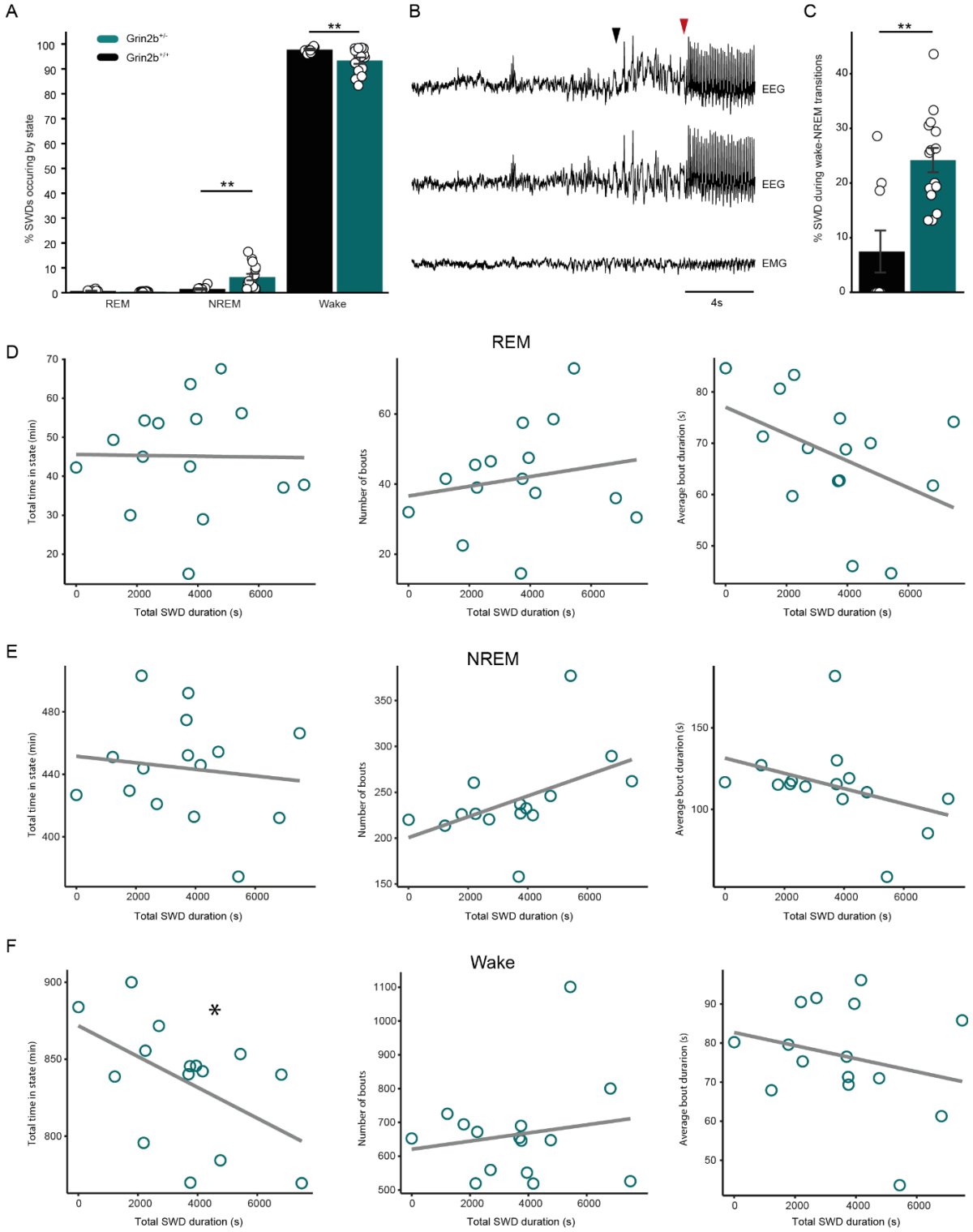

Figure 5 SWDs preferentially occur during wake but sleep abnormalities do not correlate with SWDs in Grin2b$^{+/-}$ animals. *(**A**) Plot of average percentage of SWDs occurring during REM, NREM and wake brain states. Compared to wild-type littermates, Grin2b$^{+/-}$ rats have less SWDs in wake and more SWDs in NREM (genotype P = 0.98, state P < 0.00001, genotype x state P = 0.00008 (wake P = 0.0022, NREM P = 0.0011), Two-way ANOVA with Tukey post hoc tests). Bars indicate mean values (mean ± SEM). Points correspond to values from individual rats. (**B**) Representative EEG and EMG voltage traces during a wake-NREM transition with a SWD. Black arrowhead indicates start of NREM and red arrowhead indicates start of SWD. (**C**) A higher proportion of SWDs in NREM initiate during wake-NREM transitions*

*in Grin2b$^{+/-}$ when compared to wild-type animals (P = 0.0052, Wilcoxon rank sum test). Bars indicate mean values (mean ± SEM). Points correspond to values from individual rats. Correlation plots of total time in state (left), number of bouts (middle) and average bout duration (right) with SWD duration for REM (**D**), NREM (**E**) and wake (**F**), plotted against total SWD duration. Quantification revealed total SWD duration is negatively correlated to total time awake (P = 0.048, Pearson correlation) and uncorrelated to all other sleep measurements (see results section for detailed statistics). Points correspond to values from individual rats.*

We next determined whether there was a correlation between the time spent in SWDs and abnormalities in *Grin2b*$^{+/-}$ sleep-wake rhythms. Total seizure durations in *Grin2b*$^{+/-}$ animals correlated with total time in wake (Pearson correlation, T = -2.16, DF = 13, R = -0.51, P = 0.048; Fig 5F), but not with total time in REM (Pearson correlation, T = -0.055, DF = 13, R = -0.015, P = 0.96; Fig. 5D) and NREM sleep (Pearson correlation, T = -1.47, DF = 13, R = -0.13, P = 0.65; Fig. 5F). There was also no correlation between total SWD duration and bouts of REM (Pearson correlation, T = 0.704, DF = 13, R = -0.19, P = 0.49; Fig. 5D), NREM (Pearson correlation, T = 2.006, DF = 13, R = 0.49, P = 0.066; Fig. 5E) and wake (Pearson correlation, T = 0.61, DF = 13, R = 0.17, P = 0.55; Fig. 5F), as well as average bout duration of REM (Pearson correlation, T = 0.61, DF = 13, R = 0.17, P = 0.55; Fig. 5D), NREM (Pearson correlation, T = -1.44, DF = 13, R = -0.37, P = 0.17; Fig. 5E) and wake (Pearson correlation, T = -0.93, DF = 13, R = -0.25, P = 0.37; Fig. 5F). The general lack of correlation between SWDs and sleep abnormalities in *Grin2b*$^{+/-}$ suggests that the two phenotypes have independent underlying mechanisms.

Pharmacological blockade of SWDs

We next evaluated whether SWDs in *Grin2b*$^{+/-}$ and *Grin2b*$^{+/+}$ rats could be suppressed pharmacologically. We tested the efficacy of ethosuximide, a T-type voltage-gated calcium channel blocker used in the treatment of absence seizures in humans[35] and known to block SWDs in other absence seizure rodent models.[36] We also evaluated seizure responses to memantine, a noncompetitive NMDAR antagonist currently explored as a mono or adjunctive treatment option in NMDAR related epilepsies.[1,37–39] As *Grin2b*$^{+/-}$ rats had a more severe seizure phenotype, we hypothesized that altered NMDAR-mediated signalling may contribute to brain circuits underlying SWDs and that blocking NMDARs would therefore reduce SWD activity.

We found that in both *Grin2b*$^{+/-}$ and *Grin2b*$^{+/+}$ rats, systemic ethosuximide resulted in significantly less SWDs than memantine and saline (Mixed effects ANOVA, effect of treatment F = 6.48, DF = 2, P = 0.0049; genotype F = 0.42, DF = 1, P = 0.53; treatment x genotype F = 0.34, DF = 2, P = 0.71; Tukey *post hoc* test, ethosuximide-saline P = 0.0081, ethosuximide-memantine P = 0.015, , memantine-saline P = 0.96, Fig. 6B). Both ethosuximide and memantine, however, were effective in significantly reducing the average duration of SWDs in *Grin2b*$^{+/-}$ but not *Grin2b*$^{+/+}$ animals (Mixed effects ANOVA, effect of treatment F = 9.17, DF = 2, P = 0.00048; genotype F = 0.71, DF = 1, P = 0.41; treatment x genotype F = 3.34, DF = 2, P = 0.044; Tukey *post hoc* test, ethosuximide-saline P < 0.0001, memantine-saline P = 0.0002, memantine-ethosuximide P = 0.39, Fig. 6C). The specific effect on *Grin2b*$^{+/-}$ rats, but not wild-types, suggests that the mechanisms of underlying seizures may be different between genotypes. Furthermore, memantine's effect on reducing SWD duration, but not affecting SWD occurrence, may be due to its use-dependent mechanism of action, requiring opening of the channel to get access to the channel pore, which only happens after seizures begin.[40] The combined effect of less SWDs with lower duration likely resulted in ethosuximide, but not memantine, reducing total seizure durations in both rat groups (Mixed effects ANOVA, effect of treatment F = 9.44, DF = 2, P = 0.0011; genotype F = 0.67, DF = 1, P = 0.43; treatment x

genotype F = 1.15, DF = 2, P = 0.34; Tukey *post hoc* test, ethosuximide-saline P = 0.0005, ethosuximide-memantine P = 0.083, memantine-saline P = 0.98; Fig. 6D). Both ethosuximide and memantine could therefore potentially be tested as treatments for SWDs in *GRIN2B* patients.

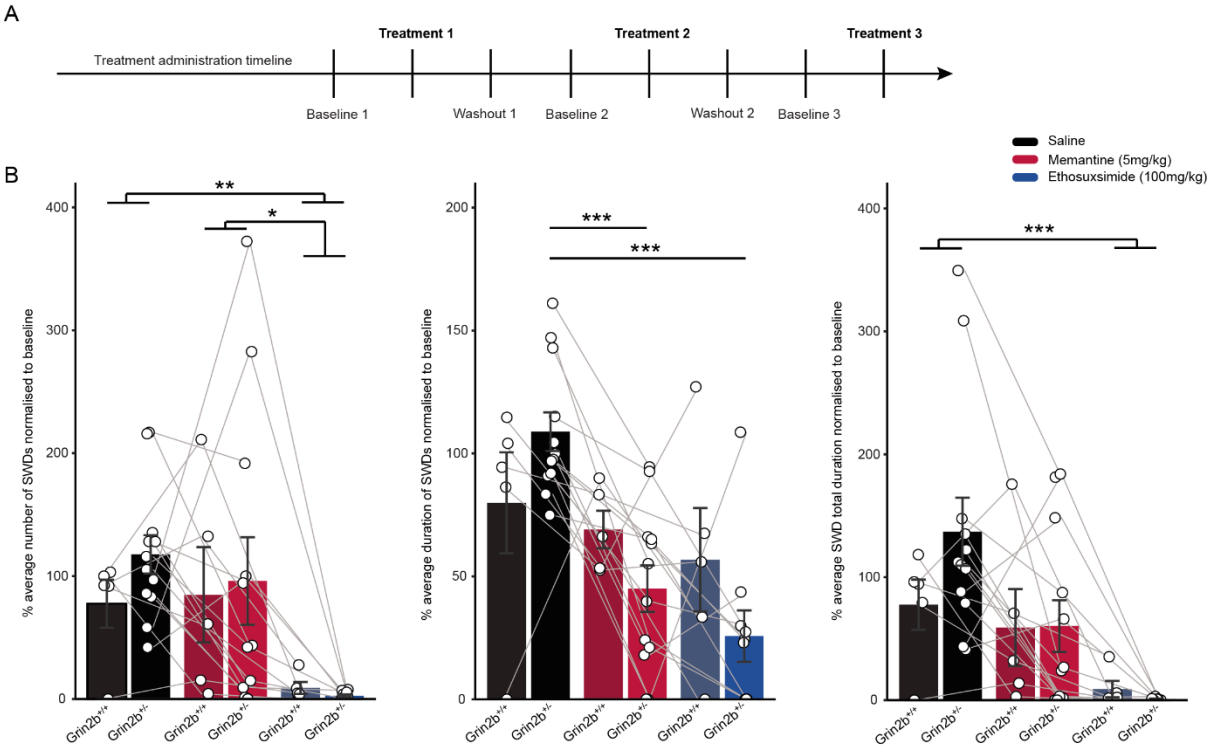

Figure 6 Acute administration of anti-seizure drugs attenuates SWDs. *(**A**) Diagram of pharmacology experiment timeline. Panels showing effects of acute drug treatment on SWD average number (**B**), average duration (**C**) and total duration (**D**) of SWDs in Grin2b$^{+/-}$ and wild-type animals. Treatment with ethosuximide successfully blocked SWD events in both groups (treatment P = 0.0049 (ethosuximide-saline P = 0.0081, ethosuximide-memantine P = 0.015), genotype P = 0.53, treatment x genotype P = 0.71, Mixed effects ANOVA with Tukey post hoc tests) (**B**). Memantine and ethosuximide reduced average SWD duration in Grin2b$^{+/-}$ rats (treatment P = 0.00048, genotype P = 0.71, treatment x genotype P = 0.044 (ethosuximide-saline P < 0.0001, memantine-saline P = 0.0002), Mixed effects ANOVA with Tukey post hoc tests) (**C**). Total seizure duration was also significantly reduced following ethosuximide treatment in both Grin2b$^{+/-}$ and wild-type rats (treatment P = 0.0011 (ethosuximide-saline P = 0.0005), genotype P = 0.43, treatment x genotype P = 0.34, Mixed effects ANOVA with Tukey post hoc tests) (**D**), see results for detailed statistics. Bars indicate mean values (mean ± SEM). Points correspond to values from individual rats and grey lines follow treatment response of each individual rat.*

Discussion

We identify clinically relevant epilepsy and sleep-wake phenotypic abnormalities in a novel model of *GRIN2B* haploinsufficiency. *Grin2b*$^{+/-}$ animals had a 50 % reduction in *GRIN2B* expression compared to wild-type levels both in the somatosensory cortex and the hippocampus in adult rats. We show that *Grin2b*$^{+/-}$ rats displayed a higher prevalence of absence seizure SWDs, which had increased spectral power, throughout both light and dark phases of the 24-hour cycle. Sleep-wake distributions were disrupted in mutant animals, although the occurrence of SWDs was largely uncorrelated to the severity of sleep-wake abnormalities. Finally, we found that pharmacological treatment with ethosuximide was able

to both reduce the number and average duration of absence seizures while memantine only reduced average SWD duration. However, both drugs reduced absence seizure durations only in *Grin2b*$^{+/-}$ animals and not wild-types, suggesting different mechanism for seizure generation. Both drugs are approved for clinical use and could prove to be translationally relevant options.

Although absence seizures are not the most prominent seizure type amongst patients with *GRIN2B* mutations, they have been reported in some individuals with loss of function variants.[2] We showed that *Grin2b*$^{+/-}$ rats had a higher number of absence seizures, which were significantly longer in duration and had higher spectral power when compared to wild-type littermates. Over 24 hours, *Grin2b*$^{+/-}$ mutants had a total of 3598 seconds of SWDs, almost an entire hour of the day in an absence seizure. In contrast, wild-type littermates had day average totals of less than a minute. The increased duration in the observed seizure phenotype, suggests SWDs in *Grin2b*$^{+/-}$ animals may resemble atypical absence seizures in patients, which are characteristically longer and are associated with epileptic encephalopathies such as Lennox-Gastaut syndrome.[41,42]

Increased cortical excitation is thought to trigger SWDs.[21,43–45] Activity spreads to thalamic structures and generalises bilaterally through various thalamocortical circuits.[46] The two-fold decrease in Glun2B expression observed in *Grin2b*$^{+/-}$ rats likely alters thalamocortical synaptic dynamics and connectivity, as other mutations that change physiological synaptic transmission have been shown to modulate the brain circuitry mediating SWDs. For example, decreased AMPAR-mediated excitatory transmission in stargazer and *GRIA4* knockout mice at corticothalamic synapses projecting to reticular thalamic nucleus, which is thought to pace corticothalamic rhythmic oscillations, results in diminished feedforward reticular thalamic inhibition and SWDs.[47–49] Deficits in inhibitory synaptic transmission, specifically at reticular thalamic-thalamic GABAerigic terminals underlies SWDs in a *NLGN2* knockout mouse model[50], while mice with selective loss of the *SCN8A* gene in inhibitory neurons, display deficits in intrinsic intra-reticular excitatory output, leading to excessive burst firing and the emergence of SWDs.[51]

In the context of *GRIN2B*, a recent publication showed that in utero electroporation of a *GRIN2B* loss of function truncating variant resulted in reduced GluN2B surface expression and NMDAR hypofunction in rat hippocampal tissue, which in adult rats manifested as core ASD behavioural phenotypes and an enhanced risk of pentylenetetrazol-induced seizures.[52] NMDAR hypofunction is also observed in hippocampal tissue from *SHANK-2* knockout mice and in transfected rat cortical neurons null for *SHANK-3*. In both cases excitation-inhibition network dynamics are altered and *SHANK-2* knockout mice also exhibit ASD-like impairments in social interactions, as well as repetitive behaviours.[53,54] Such pathological shifts in network excitation-inhibition ratios are hallmark of ASD, epilepsy and neurodevelopmental disorders[55,56] and *GRIN2A* variants that decrease NMDAR activation are reported in individuals with developmental delay and severe epilepsy.[57] This implies that similarly to the above, *GRIN2B* haploinsufficiency could contribute to NMDAR hypofunction and seizure pathogenesis in *Grin2b*$^{+/-}$ animals.

Dysfunctional sleep is commonly observed in children and adults with neurodevelopmental disorders and severe sleep fragmentation and difficulties falling asleep have been reported in individuals with pathological *GRIN2B* variants.[1,5,9] REM, NREM and wake brain states were all significantly altered in *Grin2b*$^{+/-}$ rats. Despite a slight increase in the average duration of individual REM epochs, there was a striking reduction in total REM minutes over the 24-hour cycle. The reduced net REM was underpinned by a lower occurrence of REM bouts in *GRIN2B* heterozygous knockouts and may indicate altered REM initiation mechanisms. Total NREM minutes were unchanged over 24 hours but *Grin2b*$^{+/-}$ rats had fewer NREM bouts that were

longer in duration. Finally, wake total minutes over 24 hours were also slightly increased in mutants, which was mediated by clear increases in the number of wake bouts, despite a decrease in their average duration.

Sleep modulation and diurnal rhythmicity are in part driven by NMDAR-dependent processes, and in rats, NMDAR activation has been shown to strongly alter light-dark locomotor and social behaviour transitions conductive to sleep-wake physiology.[58] Although circadian regulation of sleep and sleep homeostasis does not begin to emerge until postnatal day 17[59], after possible NMDAR functional compensation by Glun2A, it was recently shown that NMDAR mediated sleep drive specifically requires phosphorylation of Glun2B subunits.[60] Additionally, Glun2B is the dominant NMDAR subunit mediating extracellular signal-regulated kinase 1/2 cascade activity, which is known to regulate sleep-wake distribution and NREM sleep duration.[61] Mitogen-activated protein kinases phosphorylate core clock gene regulators[62–67], and these pathways are affected in *SYNGAP1*, *NLGN3*, *FMR1* and *SCN2A* deficient mice and rats [68–71], which also present with sleep impairments.[22,70,72,73] Thus, inadequate GluN2B cellular signalling could in part contribute to the sleep alterations observed in *Grin2b*$^{+/-}$ mutants. Future work will need to investigate whether dysregulation in diurnal behavioural patterns is present, and whether and to what extent mitogen-activated protein kinase activity and clock gene modulation is affected by GluN2B haploinsufficiency. Collectively these data suggest a compromised sleep architecture in this model, which is consistent with clinical reports, and to our knowledge, offers the first pre-clinical quantitative evidence of dysfunctional sleep patterns relating to *GRIN2B* haploinsufficiency.

We found no correlation between REM and NREM sleep abnormalities and total SWD activity. This suggest *GRIN2B* haploinsufficiency may differentially impact brain circuits mediating absence seizure and networks underlying sleep-wake physiology. SWDs primarily occurred when *Grin2b*$^{+/-}$ rats were awake and interestingly, absence seizures were more likely to initiate during wake-NREM transitions in *Grin2b*$^{+/-}$ rats compared to wild-type controls, which could result in the reduced amount NREM bouts observed in mutant animals. Quiet-restful wake and NREM are states in which absence seizures occur more frequently in Long Evans rats, with a high probability of SWDs occurring around wake to NREM transitions[74], when thalamic synchrony is increased.[34] Our data suggests that the mechanisms mediating wake-sleep transition in *Grin2b*$^{+/-}$ animals are functioning abnormally and may be a result of hypersynchronous activation in NREM initiating circuits.

Finally, we found SWDs in *Grin2b*$^{+/-}$ rats were sensitive to systemic treatment with ethosuximide and memantine. Ethosuximide is one of most widely used drugs for the treatment of absence seizures, and as in our study, successfully diminishes SWDs in rodent models and patients.[75–78] We found memantine had no effect on the frequency of occurrence of SWDs, but did however, decrease their average duration. This effect may be due memantine's action at the NMDAR magnesium binding site, which is only exposed during periods of membrane depolarization.[39,79] Consequently, absence seizure initiation may remain unaffected but, after successive bouts of membrane depolarization during a SWD, the events may shorten when memantine blocks the receptor at the magnesium site. Generally, the effectiveness of memantine on drug-resistant early-onset epilepsy in individuals with gain of function *GRIN2* variants (*GRIN2A*, *GRIN2B* and *GRIN2D*) is mixed[1,80–82] and memantine treatment did not improve seizure frequency in four patients with *GRIN2B* gain of function mutations.[1] Despite this, to our knowledge use of memantine has not been documented in patients with loss of function mutations, and our results suggest that the compound could potentially have favourable outcomes if extended to the treatment of seizures in patients with loss of function variants, or as an adjunctive therapy.

In conclusion, we report on absence seizure and abnormal sleep phenotypes in a novel rat model of *GRIN2B* haploinsufficiency. Additionally, we demonstrate seizures in *Grin2b*$^{+/-}$ animals are sensitive to ethosuximide and memantine and propose both drugs could favourably impact on absence seizure severity. These data are consistent with clinical observations and as such provide a translationally relevant tool for future research that should aim at defining the underlying pathological mechanisms and developing targeted therapeutics for *GRIN2B* related disorders.

References

1. Platzer K, Yuan H, Schütz H, et al. *GRIN2B* encephalopathy: novel findings on phenotype, variant clustering, functional consequences and treatment aspects. *J Med Genet*. 2017;54(7):460-470.

2. Epi4K Consortium. EPProject. De novo mutations in epileptic encephalopathies. *Nature*. 2013;501(7466):217-221.

3. Endele S, Rosenberger G, Geider K, et al. Mutations in GRIN2A and GRIN2B encoding regulatory subunits of NMDA receptors cause variable neurodevelopmental phenotypes. *Nat Genet*. 2010;42(11):1021-1026.

4. O'Roak BJ, Deriziotis P, Lee C, et al. Exome sequencing in sporadic autism spectrum disorders identifies severe de novo mutations. *Nat Genet*. 2011;43(6):585-589.

5. Freunscht I, Popp B, Blank R, et al. Behavioral phenotype in five individuals with de novo mutations within the GRIN2B gene. *Behavioral and Brain Functions*. 2013;9(1):20.

6. Smigiel R, Kostrzewa G, Kosinska J, et al. Further evidence for *GRIN2B* mutation as the cause of severe epileptic encephalopathy. *Am J Med Genet A*. 2016;170(12):3265-3270.

7. Lemke JR, Hendrickx R, Geider K, et al. *GRIN2B* mutations in west syndrome and intellectual disability with focal epilepsy. *Ann Neurol*. 2014;75(1):147-154.

8. Scheffer IE, Berkovic S, Capovilla G, et al. ILAEclassification of the epilepsies: Position paper of the ILAECommission for Classification and Terminology. *Epilepsia*. 2017;58(4):512-521.

9. Simons Searchlight. Simons Searchlight Registry Update GRIN2B, 2021. https://cdn.simonssearchlight.org/wpcontent/uploads/2021/10/20043802/GRIN2B_Q3.pdf

10. Lemke JR. Predicting incidences of neurodevelopmental disorders. *Brain*. 2020;143(4):1046-1048.

11. Traynelis SF, Wollmuth LP, McBain CJ, et al. Glutamate receptor ion channels: structure, regulation, and function. *Pharmacol Rev*. 2010;62(3):405-496.

12. Paoletti P, Bellone C, Zhou Q. NMDA receptor subunit diversity: impact on receptor properties, synaptic plasticity and disease. *Nat Rev Neurosci*. 2013;14(6):383-400.

13. Wyllie DJA, Livesey MR, Hardingham GE. Influence of GluN2 subunit identity on NMDA receptor function. *Neuropharmacology*. 2013;74:4-17.

14. Kellner S, Abbasi A, Carmi I, et al. Two de novo GluN2B mutations affect multiple NMDAR-functions and instigate severe pediatric encephalopathy. *Elife*. 2021;10.

15. Jiang H, Jiang W, Zou J, et al. The GluN2B subunit of N-methy-D-asparate receptor regulates the radial migration of cortical neurons in vivo. *Brain Res*. 2015;1610:20-32.

16. Sceniak MP, Fedder KN, Wang Q, et al. A GluN2B mutation identified in Autism prevents NMDA receptor trafficking and interferes with dendrite growth. *J Cell Sci*. 2019;132(20).

17. Bahry JA, Fedder-Semmes KN, Sceniak MP, Sabo SL. An Autism-Associated de novo Mutation in GluN2B Destabilizes Growing Dendrites by Promoting Retraction and Pruning. *Front Cell Neurosci*. 2021;15.

18. Liu S, Zhou L, Yuan H, et al. A Rare Variant Identified Within the GluN2B C-Terminus in a Patient with Autism Affects NMDA Receptor Surface Expression and Spine Density. *The Journal of Neuroscience*. 2017;37(15):4093-4102.

19. Dunkley PR, Jarvie PE, Robinson PJ. A rapid Percoll gradient procedure for preparation of synaptosomes. *Nat Protoc*. 2008;3(11):1718-1728.

20. Jiang Z, Huxter JR, Bowyer SA, et al. TaiNi: Maximizing research output whilst improving animals' welfare in neurophysiology experiments. *Sci Rep*. 2017;7(1):8086.

21. Meeren HKM, Pijn JPM, Van Luijtelaar ELJM, Coenen AML, Lopes da Silva FH. Cortical Focus Drives Widespread Corticothalamic Networks during Spontaneous Absence Seizures in Rats. *The Journal of Neuroscience*. 2002;22(4):1480-1495.

22. Buller-Peralta I, Maicas-Royo J, Lu Z, et al. Abnormal brain state distribution and network connectivity in a *SYNGAP1* rat model. *Brain Commun*. 2022;4(6).

23. Katsanevaki D, Till S, Buller-Peralta I, et al. Heterozygous deletion of SYNGAP enzymatic domains in rats causes selective learning, social and seizure phenotypes. *bioRxiv*. [Preprint] doi:https://doi.org/10.1101/2020.10.14.339192

24. Madrid-López N, Estrada J, Díaz J, Bassi A, Délano PH, Ocampo-Garcés A. The Sleep–Wake Cycle in the Nicotinic Alpha-9 Acetylcholine Receptor Subunit Knock-Out Mice. *Front Cell Neurosci*. 2017;11.

25. Rahim KJ, Burr WS, Thomson DJ. *Applications of Multitaper Spectral Analysis to Nonstationary Data*. PhD thesis. Queen's University; 2014.

26. R Core Team. R: A Language and Environment for Statistical Computing. 2022. https://www.R-project.org

27. van Brakel JPG. Robust peak detection algorithm using z-scores. Published online 2014. https://stackoverflow.com/questions/22583391/peak-signal-detection-in-realtime-timeseries-data/22640362#22640362

28. Fasol MCM, Escudero J, Gonzalez-Sulser A. Single-Channel EEG Artifact Identification with the Spectral Slope. *bioRxiv*. [Preprint] https://doi.org/10.1101/2023.11.12.566749

29. McHugh ML. Interrater reliability: the kappa statistic. *Biochem Med (Zagreb)*. 2012;22(3):276-282.

30. Posit team. RStudio: Integrated Development Environment for R. 2022. http://www.posit.co

31. Fox J, Weisberg S. *An R Companion to Applied Regression*. Third. Sage; 2019.

32. Kuznetsova A, Brockhoff PB, Christensen RHB. lmerTest Package: Tests in Linear Mixed Effects Models. *J Stat Softw*. 2017;82(13).

33. Wickham H. Data Analysis. In: *ggplot2. Use R!*. Springer. Cham; 2016:189-201.

34. Halassa MM, Chen Z, Wimmer RD, et al. State-Dependent Architecture of Thalamic Reticular Subnetworks. *Cell*. 2014;158(4):808-821.

35. Zimmerman FT, Burgemeister BB. A new drug for petit mal epilepsy. *Neurology*. 1958;8(10):769-769.

36. Terzioglu B, Aypak C, Onat FY, Küçükibrahimoglu E, Özkaynakçi AE, Gören MZ. The Effects of Ethosuximide on Amino Acids in Genetic Absence Epilepsy Rat Model. *J Pharmacol Sci*. 2006;100(3):227-233.

37. Bormann J. Memantine is a potent blocker of N-methyl-D-aspartate (NMDA) receptor channels. *Eur J Pharmacol*. 1989;166(3):591-592.

38. Parsons CG, Danysz W, Quack G. Memantine is a clinically well tolerated N-methyl-d-aspartate (NMDA) receptor antagonist—a review of preclinical data. *Neuropharmacology*. 1999;38(6):735-767.

39. Chen HS, Lipton SA. Mechanism of memantine block of NMDA-activated channels in rat retinal ganglion cells: uncompetitive antagonism. *J Physiol*. 1997;499(1):27-46.

40. Parsons CG, Gruner R, Rozental J, Millar J, Lodge D. Patch clamp studies on the kinetics and selectivity of N-methyl-d-aspartate receptor antagonism by memantine (1-amino-3,5-dimethyladamantan). *Neuropharmacology*. 1993;32(12):1337-1350.

41. Arzimanoglou A, French J, Blume WT, et al. Lennox-Gastaut syndrome: a consensus approach on diagnosis, assessment, management, and trial methodology. *Lancet Neurol*. 2009;8(1):82-93.

42. Meritam Larsen P, Wüstenhagen S, Terney D, Gardella E, Aurlien H, Beniczky S. Duration of epileptic seizure types: A data-driven approach. *Epilepsia*. 2023;64(2):469-478.

43. Pumain R, Louvel J, Gastard M, Kurcewicz I, Vergnes M. Responses to N-methyl-D-aspartate are enhanced in rats with Petit Mal-like seizures. In: *Generalized Non-Convulsive Epilepsy: Focus on GABA-B Receptors*. *J Neural Transm* (suppl). 1992; 35:97-108.

44. Polack PO, Guillemain I, Hu E, Deransart C, Depaulis A, Charpier S. Deep Layer Somatosensory Cortical Neurons Initiate Spike-and-Wave Discharges in a Genetic Model of Absence Seizures. *Journal of Neuroscience*. 2007;27(24):6590-6599.

45. Studer F, Laghouati E, Jarre G, David O, Pouyatos B, Depaulis A. Sensory coding is impaired in rat absence epilepsy. *J Physiol*. 2019;597(3):951-966.

46. Crunelli V, Lőrincz ML, McCafferty C, et al. Clinical and experimental insight into pathophysiology, comorbidity and therapy of absence seizures. *Brain*. 2020;143(8):2341-2368.

47. Menuz K, Nicoll RA. Loss of Inhibitory Neuron AMPA Receptors Contributes to Ataxia and Epilepsy in *Stargazer* Mice. *The Journal of Neuroscience*. 2008;28(42):10599-10603.

48. Barad Z, Shevtsova O, Arbuthnott GW, Leitch B. Selective loss of AMPA receptors at corticothalamic synapses in the epileptic stargazer mouse. *Neuroscience*. 2012;217:19-31.

49. Paz JT, Bryant AS, Peng K, et al. A new mode of corticothalamic transmission revealed in the Gria4−/− model of absence epilepsy. *Nat Neurosci*. 2011;14(9):1167-1173.

50. Cao F, Liu JJ, Zhou S, et al. Neuroligin 2 regulates absence seizures and behavioral arrests through GABAergic transmission within the thalamocortical circuitry. *Nat Commun*. 2020;11(1):3744.

51. Makinson CD, Tanaka BS, Sorokin JM, et al. Regulation of Thalamic and Cortical Network Synchrony by Scn8a. *Neuron*. 2017;93(5):1165-1179.e6.

52. Wang X, Guo Z, Mei D, et al. The GluN2B-Trp373 NMDA Receptor Variant is Associated with Autism-, Epilepsy-Related Phenotypes and Reduces NMDA Receptor Currents in Rats. *Neurochem Res*. 2022;47(6):1588-1597.

53. Duffney LJ, Wei J, Cheng J, et al. Shank3 Deficiency Induces NMDA Receptor Hypofunction via an Actin-Dependent Mechanism. *The Journal of Neuroscience*. 2013;33(40):15767-15778.

54. Won H, Lee HR, Gee HY, et al. Autistic-like social behaviour in Shank2-mutant mice improved by restoring NMDA receptor function. *Nature*. 2012;486(7402):261-265.

55. Bozzi Y, Provenzano G, Casarosa S. Neurobiological bases of autism–epilepsy comorbidity: a focus on excitation/inhibition imbalance. *European Journal of Neuroscience*. 2018;47(6):534-548.

56. Rubenstein JLR, Merzenich MM. Model of autism: increased ratio of excitation/inhibition in key neural systems. *Genes Brain Behav*. 2003;2(5):255-267.

57. Gao K, Tankovic A, Zhang Y, et al. A de novo loss-of-function GRIN2A mutation associated with childhood focal epilepsy and acquired epileptic aphasia. *PLoS One*. 2017;12(2):e0170818.

58. Burgdorf JS, Vitaterna MH, Olker CJ, et al. NMDAR activation regulates the daily rhythms of sleep and mood. *Sleep*. 2019;42(10).

59. Frank MG, Ruby NF, Heller HC, Franken P. Development of Circadian Sleep Regulation in the Rat: A Longitudinal Study Under Constant Conditions. *Sleep*. 2017;40(3).

60. Wang Z, Ma J, Miyoshi C, et al. Quantitative phosphoproteomic analysis of the molecular substrates of sleep need. *Nature*. 2018;558(7710):435-439.

61. Mikhail C, Vaucher A, Jimenez S, Tafti M. ERK signaling pathway regulates sleep duration through activity-induced gene expression during wakefulness. *Sci Signal*. 2017;10(463).

62. Hirayama J, Cardone L, Doi M, Sassone-Corsi P. Common pathways in circadian and cell cycle clocks: Light-dependent activation of Fos/AP-1 in zebrafish controls CRY-1a and WEE-1. *Proceedings of the National Academy of Sciences*. 2005;102(29):10194-10199.

63. Karin M. The Regulation of AP-1 Activity by Mitogen-activated Protein Kinases. *Journal of Biological Chemistry*. 1995;270(28):16483-16486.

64. Tao W, Wu J, Zhang Q, et al. EGR1 regulates hepatic clock gene amplitude by activating Per1 transcription. *Sci Rep*. 2015;5(1):15212.

65. Yap EL, Greenberg ME. Activity-Regulated Transcription: Bridging the Gap between Neural Activity and Behavior. *Neuron*. 2018;100(2):330-348.

66. Coogan AN, Piggins HD. Circadian and Photic Regulation of Phosphorylation of ERK1/2 and Elk-1 in the Suprachiasmatic Nuclei of the Syrian Hamster. *The Journal of Neuroscience*. 2003;23(7):3085-3093.

67. El Gaamouch F, Buisson A, Moustie O, et al. Interaction Between CaMKII and GluN2B Controls ERK-Dependent Plasticity. *Journal of Neuroscience*. 2012;32(31):10767-10779.

68. Gkogkas CG, Khoutorsky A, Cao R, et al. Pharmacogenetic Inhibition of eIF4E-Dependent Mmp9 mRNA Translation Reverses Fragile X Syndrome-like Phenotypes. *Cell Rep*. 2014;9(5):1742-1755.

69. Hörnberg H, Pérez-Garci E, Schreiner D, et al. Rescue of oxytocin response and social behaviour in a mouse model of autism. *Nature*. 2020;584(7820):252-256.

70. Ma Z, Eaton M, Liu Y, et al. Deficiency of autism-related Scn2a gene in mice disrupts sleep patterns and circadian rhythms. *Neurobiol Dis*. 2022;168:105690.

71. Komiyama NH, Watabe AM, Carlisle HJ, et al. SynGAP Regulates ERK/MAPK Signaling, Synaptic Plasticity, and Learning in the Complex with Postsynaptic Density 95 and NMDA Receptor. *The Journal of Neuroscience*. 2002;22(22):9721-9732.

72. Boone CE, Davoudi H, Harrold JB, Foster DJ. Abnormal Sleep Architecture and Hippocampal Circuit Dysfunction in a Mouse Model of Fragile X Syndrome. *Neuroscience*. 2018;384:275-289.

73. Thomas AM, Schwartz MD, Saxe MD, Kilduff TS. Sleep/Wake Physiology and Quantitative Electroencephalogram Analysis of the Neuroligin-3 Knockout Rat Model of Autism Spectrum Disorder. *Sleep*. 2017;40(10).

74. Kozák G, Földi T, Berényi A. Spike-and-Wave Discharges Are Not Pathological Sleep Spindles, Network-Level Aspects of Age-Dependent Absence Seizure Development in Rats. *eNeuro*. 2020;7(1):ENEURO.0253-19.2019.

75. Glauser TA, Cnaan A, Shinnar S, et al. Ethosuximide, valproic acid, and lamotrigine in childhood absence epilepsy: Initial monotherapy outcomes at 12 months. *Epilepsia*. 2013;54(1):141-155.

76. Richards DA, Manning JPA, Barnes D, et al. Targeting thalamic nuclei is not sufficient for the full anti-absence action of ethosuximide in a rat model of absence epilepsy. *Epilepsy Res*. 2003;54(2-3):97-107.

77. Penovich PE, James Willmore L. Use of a new antiepileptic drug or an old one as first drug for treatment of absence epilepsy. *Epilepsia*. 2009;50(s8):37-41.

78. Taylor JA, Reuter JD, Kubiak RA, et al. Spontaneous Recurrent Absence Seizure-like Events in Wild-Caught Rats. *The Journal of Neuroscience*. 2019;39(24):4829-4841.

79. Chen H, Pellegrini J, Aggarwal S, et al. Open-channel block of N-methyl-D-aspartate (NMDA) responses by memantine: therapeutic advantage against NMDA receptor-mediated neurotoxicity. *The Journal of Neuroscience*. 1992;12(11):4427-4436.

80. Pierson TM, Yuan H, Marsh ED, et al. *GRIN2A* mutation and early-onset epileptic encephalopathy: personalized therapy with memantine. *Ann Clin Transl Neurol*. 2014;1(3):190-198.

81. XiangWei W, Jiang Y, Yuan H. De novo mutations and rare variants occurring in NMDA receptors. *Curr Opin Physiol*. 2018;2:27-35.

82. Li D, Yuan H, Ortiz-Gonzalez XR, et al. GRIN2D Recurrent De Novo Dominant Mutation Causes a Severe Epileptic Encephalopathy Treatable with NMDA Receptor Channel Blockers. *The American Journal of Human Genetics*. 2016;99(4):802-816.